

Chapter 5

First-Principles Calculations of Structural, Elastic, Electronic, and Optical Properties of Pure and Tm^{2+} -Doped Alkali–Earth Chlorides MCl_2 ($M = Ca, Sr, \text{ and } Ba$)

C.-G. Ma and M.G. Brik

Abstract The structural, elastic, and electronic properties of pure and Tm^{2+} -doped alkali–earth chlorides are studied in detail using the hybrid density-functional theory as implemented in the CRYSTAL09 code. The calculated local geometrical structures of the dopant site, Mulliken populations, electronic-band structures, and density of states for the pure and doped crystals are analyzed and compared to reveal the changes induced by the impurity ion. Additionally, the electronic and optical properties of the Tm^{2+} -ions doped into alkali–earth chlorides are modeled by employing the exchange-charge model of the semi-empirical crystal-field theory with the help of the optimized local coordination structures around impurities. The successful simulation of the 4f-5d transition spectrum of Tm^{2+} ions in $SrCl_2$ is demonstrated as an example to show the validity of the combined theoretical scheme of the first-principles and crystal-field models.

C.-G. Ma (✉) · M.G. Brik (✉)
College of Sciences, Chongqing University of Posts and Telecommunications,
Chongqing 400065, People's Republic of China
e-mail: cgma.ustc@gmail.com

M.G. Brik
e-mail: mikhail.brik@ut.ee

M.G. Brik
Institute of Physics, University of Tartu, Ravila 14C, 50411 Tartu, Estonia

M.G. Brik
Institute of Physics, Jan Dlugosz University, Armii Krajowej 13/15,
42200 Czestochowa, Poland

5.1 Introduction

Rare-earth ions (or lanthanides, chemical elements from La [No. 57] to Lu [No. 71]) have been actively used for more than several decades in numerous optical applications such as phosphor materials for displays and lighting, solid-state lasers operating in various spectral regions from infrared to ultraviolet, infrared to visible up-conversion materials, etc. [1 and references therein]. The physical reason behind such a wide range of applications is that all these elements have an unfilled 4f electron shell, which is shielded from the crystalline environment by the outer completely filled 5s and 5p electron shells. A large number of energy levels, which arises from various interelectron interactions within the 4f shell, can be additionally split by a crystal field. The electronic transitions between all those energy levels cover a wide energy range and can be employed for various applications.

In a vast majority of these applications, these ions are introduced into crystalline solids in their stable trivalent state. However, there are a few lanthanide ions whose divalent state is also stable, e.g., Eu^{2+} , Tm^{2+} . One of the main differences between the trivalent and divalent lanthanides (apart from the electrical charge) is that the charge-transfer transitions and the parity allowed 5d-4f transitions of the divalent ions are located at lower energies than those of the trivalent ions; because of this they can more easily be studied experimentally. Regarding Tm^{2+} ions, it should be kept in mind that the $4f^{13}$ electron shell has only two energy levels: the ground state $^2F_{7/2}$ and the excited state $^2F_{5/2}$ located at approximately 9500 cm^{-1} [2]. As a result, the 4f-4f and 4f-5d transitions of the Tm^{2+} ions do not overlap and can be easily studied separately.

The $M\text{Cl}_2$ ($M = \text{Ca}, \text{Sr}, \text{and Ba}$) crystals are ideal candidates for studies of the spectroscopic properties of Tm^{2+} ions. First, no charge-compensation defects are required after thulium ions are introduced into these hosts. Second, there is reliable experimental information about the absorption/emission spectra of these materials [2–8]. Moreover, the earth-alkaline halides are also important from an application point of view because the laser action has been achieved in $\text{CaF}_2:\text{Tm}^{2+}$ [9]. The spectra of Tm^{2+} were modeled in our earlier publication [10].

Theoretical interpretation of peculiar features of impurity-ion spectra in crystals can be advanced by the combination of the semi-empirical crystal-field (CF) theory and the modern density-functional theory (DFT)-based computational methods. Such a combination highlights the strong features of both computational approaches and allows for creating a complementary picture of the electronic properties of doped optical materials. The short comparative list of the advantages and disadvantages of both methods is as follows: The CF theory can handle the multiplet structure of the impurity ion energy levels including low-symmetry splitting of the J manifolds and admixture of the electronic configurations of the opposite parity. These questions are beyond the current opportunities of currently used DFT-based computational packages because they are essentially based on the one-electron approximation. At the same time, the electronic-band structure of a solid simply cannot be obtained within the framework of a CF theory, whereas such calculations

are already among the standard ones in the DFT-based methods. However, from calculations of the density of states of a doped material, it is possible to locate the ground state of an impurity ion in the band gap. Determination of the ground-state position in the host band gap is a crucial issue and has decisive importance for potential applications of a given crystal with intentionally introduced impurities. After that, the energy levels of an impurity ion, calculated with the help of the CF theory, can be superimposed onto the host's band structure starting from the ground state. Such an approach was used earlier for a number of crystals doped with transition-metal and rare-earth ions [11–13].

Recently we presented an example of such consistent joint application of these two different approaches to the description of the optical properties of Tm^{2+} ions in SrCl_2 [10], and the success of such an approach was demonstrated and confirmed by good agreement between the experimental and calculated optical properties of $\text{SrCl}_2:\text{Tm}^{2+}$. This system has not been thoroughly studied so far: To illustrate such a statement, we also mention that earlier the crystal-field parameters for the 4f electrons of the Tm^{2+} ions in similar compounds of CaF_2 , SrF_2 , and BaF_2 were analyzed in Refs. [14, 15], but they were not analyzed in CaCl_2 , SrCl_2 and BaCl_2 .

Based on the above-given consideration and examples, we decided to apply the DFT-based calculations to three alkali metal halide crystals, namely, CaCl_2 , SrCl_2 , and BaCl_2 doped with Tm^{2+} ions. The structural, electronic, optical, and elastic properties of these compounds were determined using first-principles calculation: The location of the 4f and 5d energy levels of the Tm^{2+} ions in the band gaps was identified. All obtained results are compared with the experimental data (if available), and agreement between the theory and the results of the experiment is discussed.

5.2 Crystal Structure

All three compounds studied here crystallize in different space groups. The corresponding structural data are summarized in Table 5.1, whereas Fig. 5.1 depicts unit cells for each of the studied crystals as well as the local coordination structures of alkaline-earth cations.

The Ca atoms in CaCl_2 are sixfold coordinated by the chlorine ions, and the Ba and Sr atoms in BaCl_2 and SrCl_2 are eightfold and ninefold coordinated by the chlorine atoms, respectively.

As a common feature of all these crystals, we note here that the metal–chlorine distance is rather large. In CaCl_2 , there are two Ca–Cl distances of 2.704 Å and four distances of 2.765 Å. In SrCl_2 , all eight Sr–Cl bonds are equal to 3.019 Å. Finally, Ba–Cl distances in BaCl_2 vary in a wide range from 2.864 to 3.579 Å.

Table 5.1 Calculated and experimental structural data for $M\text{Cl}_2$ ($M = \text{Ca}, \text{Sr}$ and Ba) crystals

	CaCl_2 ($Pn\bar{m}m$, No. 58)		SrCl_2 ($Fm\bar{3}m$, No. 225)		BaCl_2 ($Pn\bar{m}a$, No. 62)	
	<i>Calc.</i>	<i>Exp.</i> [16]	<i>Calc.</i>	<i>Exp.</i> [17]	<i>Calc.</i>	<i>Exp.</i> [18]
a , Å	6.32847	6.24	6.97205	6.971	7.88907	7.865
b , Å	6.32626	6.43	6.97205	6.971	4.74148	4.731
c , Å	4.23826	4.2	6.97205	6.971	9.46948	9.421
$\alpha = \beta = \gamma$, °	90	90	90	90	90	90
V , Å ³	169.681	168.52	338.908	338.75	354.214	350.55
Z	2	2	4	4	4	4
M	0	0	0	0	0.251450	0.2514
	0	0	0	0	0.25	0.25
	0	0	0	0	0.117864	0.1209
Site	$2a$		$4a$		$4c$	
Cl1	0.303617	0.275	0.25	0.25	0.143961	0.1504
	0.305114	0.325	0.25	0.25	0.25	0.25
	0	0	0.25	0.25	0.429683	0.413
Site	$4g$		$8c$		$4c$	
Cl2					0.029152	0.029
					0.25	0.25
					0.829654	0.8392
Site					$4c$	

Coordinates of the crystallographic positions (in units of the lattice constants, (x, y, z) from *top* to *bottom*) of all ions are given. The symbol “ Z ” stands for the number of chemical formula units in one conventional unit cell

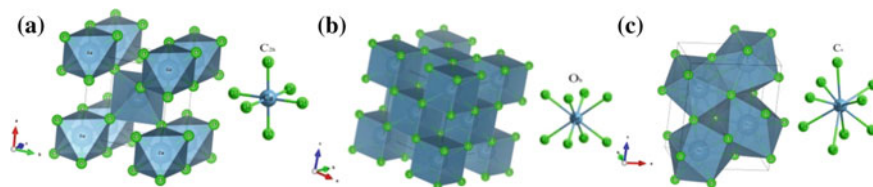


Fig. 5.1 Schematic representations for the unit cell of pure $M\text{Cl}_2$ crystal and the local coordination structure around M cation ($M = \text{Ca}$ [a], Sr [b], and Ba [c]). Drawn with VESTA [19]

5.3 Methods of Calculations

5.3.1 *Ab Initio* Calculations

The first-principles calculations of the structural, elastic, and electronic properties of pure and Tm^{2+} -doped hosts were performed using the periodic *ab initio* CRYSTAL09code [20] based on the linear combination of the atomic-orbitals

method. Closed-shell and spin-polarized calculation forms were adopted for the pure and doped systems, respectively. To achieve better agreement between the calculated and experimental properties of the considered materials and improve the description of the strongly correlated lanthanide 4f orbitals [21], we employed the hybrid exchange–correlation (EXC) functional WC1PBE consisting of a PBE correlation part and a Wu-Cohen exchange part with a fractional mixing (16 %) of the nonlocal Hartree–Fock exchange [22]. The positive performance of such a hybrid EXC functional was confirmed by our recent works [23–25]. The local Gaussian-type basis sets (BS) were chosen as follows: the all-electron BSs in the form of 86-311G and 86-511d21G were used for the Cl [26] and Ca [27] atoms, respectively; the full-relativistic effective core pseudo-potentials (ECP), i.e., ECP28MDF and ECP46MDF—together with their corresponding valence BSs from the Stuttgart/Cologne group—were applied to Sr and Ba atoms [28], respectively; for Tm atom, the inner electrons [Ar]3d¹⁰ were described by the scalar-relativistic ECP developed by Dolg et al. [29]; the other electrons 4s²4p⁶4d¹⁰5s²5p⁶4f¹³6s²5d¹ were explicitly treated by the segmented-contraction type of the valence BS (14s13p10d8f)/[10s8p5d4f] [30] related to the ECP we used; and all the primitive functions with exponents less than 0.1 bohr⁻² were excluded because it is well-known that in the LCAO calculations for crystals, the BS of a free atom must be modified because the diffuse functions may cause numerical problems due to the large overlap with the core functions of the neighboring atoms in a densely packed crystal [31].

The Monkhorst–Pack schemes for the $8 \times 8 \times 8$ and $4 \times 4 \times 4$ k -point meshes in the Brillouin zone were applied to the pure and doped cases, respectively. The truncation criteria for bielectronic integrals (Coulomb and HF exchange series) were set to 8, 8, 8, 8, and 16, and a predefined “extra extra large” pruned DFT integration grid was adopted together with much higher DFT density and grid-weight tolerances (values 8 and 16). The tolerance of the energy convergence on the self-consistent field iterations was set to 10^{-8} Hartree. The Anderson scheme with 60 % mixing was used to achieve the converged solutions for all the calculation cases, and the total spin of the doped systems was locked to a value of 1/2 in the first 15 cycles due to the single positive hole occupation in the Tm²⁺4f orbitals. In the geometry optimization with full structural relaxation, the convergence criteria of the root mean square of the gradient and the nuclear displacement were set to 0.00006 Hartree/bohr and 0.00012 bohr, respectively. For the elastic constant calculation, the default parameter values recommended in Ref. [32] were used.

5.3.2 *Crystal-Field Calculations and Exchange-Charge Model*

The parameterized effective Hamiltonians for the 4f¹³ and 4f¹²5d configurations of Tm²⁺ ions can be respectively written as:

$$\mathbf{H}(4f^{13}) = \mathbf{E}_{\text{avg}} + \zeta_f A_{so}(f) + \mathbf{H}_{CF}(4f) \quad (1)$$

$$\begin{aligned} \mathbf{H}(4f^{12}5d) = & \Delta_E(\text{fd}) + \sum_{k=2,4} F^k(\text{fd})f_k + \sum_{j=1,3,5} G^j(\text{fd})g_j \\ & + \sum_{k=2,4,6} F^k(\text{ff})f_k + \zeta_f(\text{ff})A_{so}(\text{ff}) + \alpha(\text{ff})L(L+1) + \beta(\text{ff})G(G_2) \\ & + \gamma(\text{ff})G(R_7) + \sum_{h=0,2,4} M^h(\text{ff})m_h + \sum_{k=2,4,6} P^k(\text{ff})p_k \\ & + \zeta_d(d)A_{so}(d) + \mathbf{H}_{CF}(4f) + \mathbf{H}_{CF}(5d) \end{aligned} \quad (2)$$

where all notations and terms/operators/parameters are defined according to the standard practice [33]. The sum of all the interactions, except for the terms denoted as $\mathbf{H}_{CF}(nl)$ ($nl = 4f$ or $5d$), describes a quasi-free ion configuration Hamiltonian, the parameters of which can be taken as the free-ion ones with a reasonable reduction, caused by the nephelauxetic effect. Shortly, where E_{avg} represents the energy barycenter of the $4f^{13}$ configuration. The term denoted as $\Delta_E(\text{fd})$ is the (barycenter-to-barycenter) energy difference between both the $4f^{13}$ and the $4f^{12}5d$ configurations; the ζ_f , $\zeta_f(\text{ff})$, and $\zeta_d(d)$ entries are the spin-orbit coupling parameters for $4f$ electrons in the $4f^{13}$ configuration, $4f^{12}$ core and for the $5d$ single electron, correspondingly. The Slater radial integrals for the radial part of the electrostatic interaction among the $4f$ electrons or between the $4f$ and $5d$ electrons are denoted as $F^k(\text{ff})$ ($k = 2, 4, 6$), $F^k(\text{fd})$ ($k = 2, 4$), and $G^j(\text{fd})$ ($j = 1, 3, 5$). The two-body corrections terms describing the configuration interaction are denoted by $\alpha(\text{ff})$, $\beta(\text{ff})$, and $\gamma(\text{ff})$. Finally, the $M^h(\text{ff})$ ($h = 0, 2, 4$) and $P^k(\text{ff})$ ($k = 2, 4, 6$) are related to the spin-spin and spin-other orbit relativistic interactions and the electrostatically correlated spin-orbit interactions between $4f$ electrons, respectively (usually the ratios of $M^0:M^2:M^4$ and those of $P^2:P^4:P^6$ are kept fixed as described and explained in Ref. [34]). The last term, $\mathbf{H}_{CF}(nl)$, is the CF interaction produced by the crystal lattice ions, which is felt by the $4f$ or $5d$ electrons of rare-earth ions and leads to the splitting of the J manifolds of an impurity ion. It is a standard practice to expand this term as follows:

$$\mathbf{H}_{CF}(nl) = \sum_{k,q=-k,\dots,k} B_q^k(nl)C_q^{(k)} \quad (3)$$

where C_q^k are the spherical functions with rank k and order q defined by Wybourne [35]; and $B_q^k(nl)$ are the crystal-field parameters (CFP). The former act on the angular parts of an impurity ion's wave functions, whereas the latter reflect the local symmetry of an impurity ion's site. The CFP values can be calculated using the crystal-structure data and the exchange-charge model (ECM) as shown below. More details related to this method of calculations can be found in our recent work [36].

The choice of the quasi-free ion parameter values for the $4f^{13}$ and $4f^{12}5d$ configurations of Tm^{2+} ions was performed according to data in the earlier literature. Thus, Pan et al. [37] reported the quasi-free ion parameter values for the $4f^65d$

configuration of the Eu^{2+} ions in SrCl_2 . From their data, it is possible to obtain the reduction ratio between the free ion's values and those in the crystalline environment. The free ion-parameter values for the $4f^{N-1}5d$ configurations of $\text{Eu}^{2+}(N = 6)$ and $\text{Tm}^{2+}(N = 12)$ ions were calculated by the standard atomic-physics codes of Cowan [38, 39], and then the same reduction ratio as for the Eu^{2+} ions was directly applied to the Tm^{2+} ions. The reduced quasi-free ion parameter values for the $4f^{12}5d$ configuration of Tm^{2+} ions (using the standard notations in Ref. [33]) were obtained as follows: $F^2(\text{ff}) = 84176$, $F^4(\text{ff}) = 59189$, $F^6(\text{ff}) = 45569$, $\zeta_f(\text{ff}) = 2483$, $\alpha(\text{ff}) = 17.26$, $\beta(\text{ff}) = -624.5$, $\gamma(\text{ff}) = 1820$, $M^0(\text{ff}) = 3.81$, $P^2(\text{ff}) = 695$, $\zeta_d(\text{d}) = 1053$, $F^2(\text{fd}) = 11611$, $F^4(\text{fd}) = 5354$, $G^1(\text{fd}) = 5198$, $G^3(\text{fd}) = 4051$, and $G^5(\text{fd}) = 3056$ (all in cm^{-1}). For the $4f^{13}$ configuration of the Tm^{2+} ions, the parameter ζ_f value can be approximately taken from that of $\zeta_f(\text{ff})$. The parameters $\Delta_E(\text{fd})$ and E_{avg} are respectively adjusted to 34756 and 3912 cm^{-1} to obtain the best agreement between the experimental and calculated energy levels.

The basic ideas of the exchange-charge model of the crystal field as outlined in Ref. [40] are as follows: The CFPs of any impurity ion, i.e., $B^k q(nl)$, are represented as a sum of two different contributions that arise from the point charges of all crystal lattice ions and introduced fictitious exchange charges (placed in the space between an impurity ion and ligands) due to the spatial overlap of the impurity-ion and ligand wave functions:

$$B_q^k(nl) = -e^2 \langle nl | r^k | nl \rangle \sum_i q_i \beta_k \cdot (-1)^k C_{-q}^k(\theta_i, \varphi_i) / R_i^{k+1} \\ + e^2 \frac{2(2k+1)}{2l+1} \sum_L S_k^{nl}(R_L) \cdot (-1)^k C_{-q}^k(\theta_L, \varphi_L) / R_L \quad (4)$$

where the indexes i and L are, respectively, used to enumerate all the crystal lattice ions and the ligand ions in the nearest-neighbor coordination shell; $(R_i, \theta_i, \varphi_i)$ and $(R_L, \theta_L, \varphi_L)$ are the spherical coordinates of the i th crystal lattice ions and the L th ligand ions in the reference system centered at the Tm^{2+} ions; and the ion charges q_i for Sr and Cl atoms can be taken as +2 and -1 as the first approximation. However, in our calculations we went further and took the values of these charges from the Mulliken population analysis as obtained by the performed ab initio calculations. The reduction factor β_k ($k = 2, 4, \dots, 2l$) is defined as $1 - \sigma_k$ (the so-called shielding constant [41]) for the 4f electrons, which accounts for the screening effects produced by the outer filled 5s and 5p electron shells. However, for the 5d electrons, it is set to 1 (no screening because this is an outer orbital). The $\langle nl | r^k | nl \rangle$ entry is the radial integral of r^k (electron radial coordinate) between nl orbitals of the Tm^{2+} ions. The total overlap integral $S_k^{nl}(R_L)$ can be further expressed as:

$$S_k^{nl}(R_L) = G_s^{nl} S_s^{nl}(R_L)^2 + G_\sigma^{nl} S_\sigma^{nl}(R_L)^2 + \gamma_k^{nl} G_\pi^{nl} S_\pi^{nl}(R_L)^2 \quad (5)$$

where $\gamma_2^{4f} = 3/2$, $\gamma_4^{4f} = 1/3$, $\gamma_6^{4f} = -3/2$, $\gamma_2^{5d} = 1$, and $\gamma_4^{5d} = -4/3$ [40]; $S_s^{nl}(R_L) = \langle nl0|3s0\rangle$, $S_\sigma^{nl}(R_L) = \langle nl0|3p0\rangle$, and $S_\pi^{nl}(R_L) = \langle nl\pm 1|3p\pm 1\rangle$; and G_s^{nl} , G_σ^{nl} and G_π^{nl} entries are the dimensionless adjustable parameters. They are determined by matching the calculated energy levels of an impurity ion to the experimental positions of its three lowest in energy absorption bands. For the sake of simplicity (and this turns out to be a very good approximation indeed in most cases), these three parameters can be approximated to a single value $G(nl)$. In such a case, the value of this only parameter of the model can be easily found by matching the calculated position of the first excited state to the lowest absorption band in the experimental absorption/excitation spectrum. The moment of the nl -electron's radial coordinate r $\langle nl|r^k|nl\rangle$, as well as the overlap integrals between the nl orbitals of the Tm^{2+} ions and the outer 3s and 3p orbitals of Cl^- ions for various interionic distances, can be calculated using the corresponding numerical radial-wave functions provided by the Cowan code [38].

After all CFPs are determined, the “f-shell” program code written by M.F. Reid [33] can be employed to calculate the $4f^{13}$ and $4f^{12}5d$ CF energy levels and simulate the 4f-5d transition spectrum of Tm^{2+} ions in all considered cases. The results of these calculations are described below after the description of properties of pure $CaCl_2$, $SrCl_2$, and $BaCl_2$.

5.4 Ab Initio Calculations for Pure $CaCl_2$, $SrCl_2$, and $BaCl_2$ Crystals

The calculated structural parameters of pure MCl_2 ($M = Ca, Sr, \text{ and } Ba$) crystals are listed in Table 5.1. As seen from that table, agreement between the experimental and calculated structural characteristics is very good, especially for $SrCl_2$ and $BaCl_2$, including not only the crystal lattice constants but also the fractional coordinates of all ions in a crystal lattice. The difference between the calculated and experimental structural parameters is somewhat greater in the case of $CaCl_2$, but this can be due to the fact that the corresponding experimental data are rather old [16], and the accuracy of those measurements might not be too high (as is evidenced by the number of digits after the decimal point in the corresponding structural data).

Good agreement between the optimized and experimental structural parameters allows calculations of the electronic, optical, and elastic properties of these compounds.

Figure 5.2 shows the calculated band structures of all three studied chlorides. The common feature is that for all compounds the valence band is rather narrow (3–4 eV), whereas the conduction band is rather wide. The upper states in the valence bands are very flat, which suggests a weak dispersion of holes in the reciprocal space. The lowest states of the conduction bands are also rather flat (low mobility of electrons), except for the vicinity of the Brillouin zone center. The band

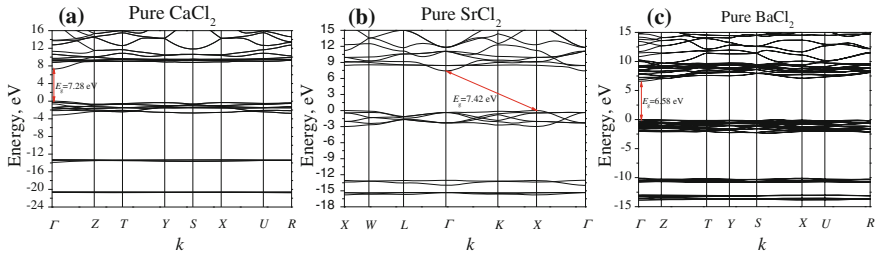


Fig. 5.2 Calculated band-structure diagrams for pure MCl_2 ($M = Ca$ [a], Sr [b], and Ba [c]) crystals. In the cases of (a) and (c), the letters Γ , Z, T, Y, S, X, U, and R stand for the high-symmetry k points (0,0,0), (0,0,1/2), (0,1/2,1/2), (0,1/2,0), (1/2,1/2,0), (1/2,0,0), (1/2,0,1/2) and (1/2,1/2,1/2), respectively, whereas the high-symmetry k points (1/2,0,1/2), (1/2,1/4,3/4), (1/2,1/2,1/2), (0,0,0) and (3/4,3/8,3/8) corresponding to the letters X, W, L, Γ and K, respectively, are chosen in the case of (b). **b** Reproduced from Ref. [10] by permission of John Wiley & Sons Ltd

gaps are direct for $CaCl_2$ and $BaCl_2$ and is indirect for $SrCl_2$. The calculated band gaps are 7.28 eV ($CaCl_2$), 7.42 eV ($SrCl_2$) and 6.58 eV ($BaCl_2$), which is in good agreement with the experimental data of 6.9 eV ($CaCl_2$), 7.5 eV ($SrCl_2$), and 7 eV ($BaCl_2$), with all experimental data taken from Ref. [42].

Composition of the calculated electronic bands can be analyzed with the help of the density-of-states (DOS) and partial-density-of-states (PDOS) diagrams shown in Fig. 5.3. The valence band in all cases is formed by the 3p states of Cl ions, whereas the conduction band is basically composed of the d states of metals (3d states of Ca, 4d states of Sr, and 5d states of Ba). These are the most important states, which determine the optical properties of these crystals. The remaining DOS peaks are located deeply in energy; they come from the completely filled 3s states of Cl and p states of metal ions and do not manifest themselves in the optical spectra.

Table 5.2 lists the calculated elastic constants for all materials. All non-zero values of the elastic constants C_{ij} (the number of these non-zero components is

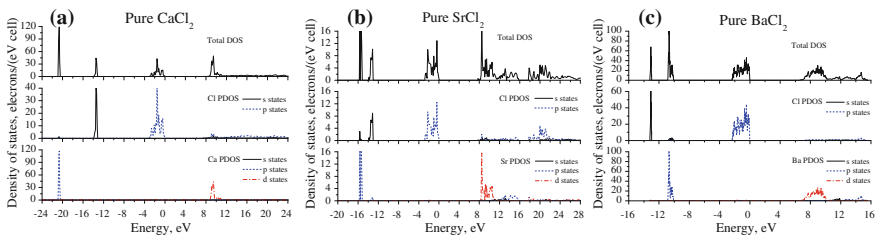


Fig. 5.3 Calculated PDOS/DOS diagrams for pure MCl_2 [$M = Ca$ (a), Sr (b) and Ba (c)] crystals. **b** Reproduced from Ref. [10] by permission of John Wiley & Sons Ltd

Table 5.2 Calculated elastic constants C_{ij} (GPa), bulk moduli B (GPa), Poisson's ratios ν , and longitudinal and transverse sound velocities $\nu_{l,t}$ (km/s) for $M\text{Cl}_2$ ($M = \text{Ca}, \text{Sr}$ and Ba) crystals

	CaCl ₂ (<i>Pnmm</i> , No. 58)	SrCl ₂ (<i>Fm</i> ³ <i>m</i> , No. 225)			BaCl ₂ (<i>Pnma</i> , No. 62)	
	This work	This work	Exp. [43]	Calc. [44]	This work	Calc. [45]
C_{11}	45.065	75.584	70.2	66	49.693	56.75
C_{12}	35.579	19.937	16.4	16	21.647	24.75
C_{13}	25.234	19.937	16.4	16	22.499	25.66
C_{22}	45.068	75.584	70.2	66	50.447	56.66
C_{23}	25.232	19.937	16.4	16	25.688	28.11
C_{33}	64.662	75.584	70.2	66	64.335	63.05
C_{44}	14.496	13.795	9.72	12	8.042	24.42
C_{55}	14.490	13.795	9.72	12	16.254	20.46
C_{66}	37.260	13.795	9.72	12	18.783	23.17
B	36.23	38.49	34.3	33	33.49	36.97
ν	0.32	0.29	0.292	0.276	0.31	0.272
ν_l	[001]	2.595	2.112		2.042	
	[010]	4.161	2.112		2.195	
	[100]	4.577	4.943		3.571	
	[111]	1.927	4.288		3.688	
ν_{l1}	[001]	2.596	2.112		1.436	
	[010]	4.577	4.943		3.598	
	[100]	4.161	2.112		2.195	
	[111]	5.559	2.735		1.857	
ν_{l2}	[001]	5.482	4.943		4.063	
	[010]	2.596	2.112		1.436	
	[100]	2.595	2.112		2.042	
	[111]	3.144	2.735		2.094	

The notation“[...]” represents the direction of sound wave propagation

determined by the crystal-lattice symmetry), bulk moduli, and Poisson's ratio—along with the sound velocities corresponding to different directions in the crystal lattices are listed in the table. Low values of the bulk moduli suggest that all three crystals are very soft substances.

Comparison of our calculated results with those available in the literature [43–45] yields good agreement between corresponding sets of data. We also went further with an analysis of the elastic anisotropy of these compounds, which can be visualized by plotting three-dimensional surfaces of the Young moduli along various directions in the crystal lattice. In the case of an orthorhombic crystal (such as CaCl₂ and BaCl₂), such a three-dimensional surface is described by the following expression [46]:

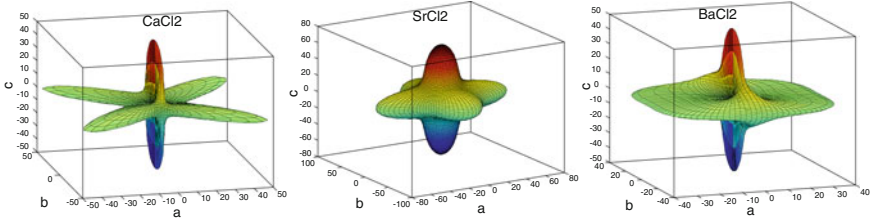


Fig. 5.4 Directional dependences of the calculated Young moduli for the $M\text{Cl}_2$ ($M = \text{Ca}, \text{Sr},$ and Ba , from *left to right*) crystals (the axes units are GPa)

$$\frac{1}{E} = l_1^4 S_{11} + 2l_1^2 l_2^2 S_{12} + 2l_1^2 l_3^2 S_{13} + l_2^4 S_{22} + 2l_2^2 l_3^2 S_{23} + l_3^4 S_{33} + l_2^2 l_3^2 S_{44} + l_1^2 l_3^2 S_{55} + l_1^2 l_2^2 S_{66}, \quad (6)$$

where E is the value of the Young's modulus in the direction determined by the direction cosines l_1, l_2, l_3 ; and S_{ij} are the elastic compliance constants, which form the matrix inverse to the matrix of the elastic constants C_{ij} . The same surface in the case of a cubic crystal (SrCl_2) is given as

$$\frac{1}{E} = S_{11} - 2 \left(S_{11} - S_{12} - \frac{1}{2} S_{44} \right) (l_1^2 l_2^2 + l_2^2 l_3^2 + l_1^2 l_3^2). \quad (7)$$

The distance from the center of such a surface to a point at its surface is equal to the Young modulus in a given direction determined by the direction cosines l_1, l_2, l_3 . Figure 5.4 shows these surfaces plotted for the studied systems, and as seen from the surfaces, the anisotropy of the elastic properties is well-pronounced, especially for CaCl_2 and BaCl_2 .

5.5 Ab Initio Calculations for Tm^{2+} -doped CaCl_2 , SrCl_2 , and BaCl_2 Crystals

Introduction of an impurity ion into a crystal can considerably change its optical properties. Even the color of a crystal can be changed because the purity-ion's energy levels, which appear in the band gap, can cause absorption in the visible range.

To model the geometrical structures of the Tm^{2+} -doped $M\text{Cl}_2$ ($M = \text{Ca}, \text{Sr},$ and Ba) crystals, we constructed three super-cells from the optimized structural data of the pure host's primitive cells by respectively using the symmetrical super-cell transformation matrices $(1 - 1 0; 1 1 0; 0 0 2)$, $(2 0 0; 0 2 0; 0 0 2)$ and $(1 - 1 0; 1 1 0; 0 0 1)$ [31]. Each studied super-cell contains eight $M\text{Cl}_2$ chemical formula units, and one M^{2+} cation was replaced by the Tm^{2+} ion. In other words, the geometry optimizations were performed on the form of $M_7\text{TmCl}_{16}$ for all cases. At first, due

Table 5.3 Calculated lattice parameters and volumes of the pure and Tm^{2+} -doped MCl_2 ($M = \text{Ca}$, Sr and Ba) supercells

	CaCl_2		SrCl_2		BaCl_2	
	Pure	Tm_{Ca}	Pure	Tm_{Sr}	Pure	Tm_{Ba}
a' , Å	8.94825	8.96384	9.85997	9.82001	9.20429	9.13257
b' , Å	8.94825	8.96384	9.85997	9.82001	9.20429	9.13257
c' , Å	8.47652	8.50451	9.85997	9.82001	9.46948	9.35929
α' , °	90	90	60	60	90	90
β' , °	90	90	60	60	90	90
γ' , °	89.9800	89.695	60	60	62.0134	62.3335
V' , Å ³	678.724	683.332	677.816	669.608	708.428	691.351
		(+0.68 %)		(-1.21 %)		(-2.41 %)

The Tm^{2+} -induced volume changes with respect to the pure host cases are given in the parentheses

to the differences in the ionic radii of the Tm^{2+} and substituted metal ions (Ca^{2+} , Sr^{2+} , and Ba^{2+}), the lattice constants and interionic distances in the doped crystal will be somewhat different from those ones for the pure host. Table 5.3 illustrates this structural difference between the pure and thulium-bearing crystals.

As seen from Table 5.3, the volume of a unit cell of CaCl_2 doped with Tm^{2+} is slightly increased (by approximately 0.68 %), whereas the unit cells of SrCl_2 and BaCl_2 undergo a compression by 1.21 and 2.41 %, respectively. Such behavior can be explained by a simple comparison of the ionic radii of all ions involved. However, inspection of the database of the ionic radii given by Shannon [47] shows that the ionic radii of Tm^{2+} ions with eightfold and ninefold coordination numbers (CN) are absent. Due to the consideration of the chemical similarity across the whole lanthanide series, we can propose a linear ionic-radius dependence of divalent lanthanide ions on their atomic number Z and coordination number N to bypass the problem we encountered above as follows:

$$R(\text{Ln}^{2+}) = 0.0521N - 0.0176Z + 1.9382 \quad (8)$$

where the values of the two slopes and the intercept were obtained by fitting the experimental data set collected in Table 5.4 [47]. The calculated ionic radius of Tm^{2+} using Eq. (8) is slightly greater than that of Ca^{2+} , but slightly smaller than those of Sr^{2+} and Ba^{2+} , as shown in Table 5.4. This straightforward equation reveals the change reason for the super-cell volume with respect to the pure-host case after Tm^{2+} -doping.

Another geometrical manifestation of doping effects is the change of characteristic interionic distance. Comparison of the $M\text{-Cl}$ ($M = \text{Ca}$, Sr , and Ba) and Tm-Cl distances in the pure and doped crystals is given by Table 5.5. Again, in accordance with the general trends in the change of the unit cell volumes from Table 5.3, the Tm-Cl distances are slightly increased, if the Tm^{2+} ions enter CaCl_2 , and decreased when the Tm^{2+} ions occupy the Sr and Ba sites in SrCl_2 and BaCl_2 , respectively.

Table 5.4 Effective ionic radii (in Å) of divalent lanthanides and M^{2+} ($M = \text{Ca}, \text{Sr}$ and Ba) cations with different CNs

CN	Nd^{2+}	Sm^{2+}	Eu^{2+}	Dy^{2+}	Tm^{2+}	Yb^{2+}	Ca^{2+}	Sr^{2+}	Ba^{2+}
6	(1.197)	(1.162)	1.17	1.07	1.03	1.02	1.00	1.18	1.35
7	(1.249)	1.22	1.20	1.13	1.09	1.08	1.06	1.21	1.38
8	1.29	1.27	1.25	1.19	(1.143)	1.14	1.12	1.26	1.42
9	1.35	1.32	1.30	(1.248)	(1.195)	(1.177)	1.18	1.31	1.47
10	(1.405)	(1.370)	1.35	(1.300)	(1.247)	(1.229)	1.23	1.36	1.52

The values obtained from the linear fitting calculation are given in the parentheses

Table 5.5 Calculated distances (in Å) from the dopant site to the chlorine ligands in the first coordination shell before and after Tm^{2+} -doping in CaCl_2 , SrCl_2 and BaCl_2 crystals

	CaCl_2		SrCl_2			BaCl_2			
M	Ca		Tm_{Ca}	Sr		Tm_{Sr}	Ba		Tm_{Ba}
Site	$\text{C}_{2\text{h}}$		$\text{C}_{2\text{h}}$	O_{h}		O_{h}	C_{s}		C_1
R	<i>Exp.</i>	<i>Calc.</i>	<i>Calc.</i>	<i>Exp.</i>	<i>Calc.</i>	<i>Calc.</i>	<i>Exp.</i>	<i>Calc.</i>	<i>Calc.</i>
Cl1	2.704	2.724	2.756	3.019	3.019	2.963	2.864	3.069	2.920
Cl2	2.704	2.724	2.756	3.019	3.019	2.963	3.167	3.081	2.829
Cl3	2.765	2.749	2.788	3.019	3.019	2.963	3.167	3.081	2.829
Cl4	2.765	2.749	2.788	3.019	3.019	2.963	3.154	3.139	2.924
Cl5	2.765	2.749	2.788	3.019	3.019	2.963	3.179	3.239	3.003
Cl6	2.765	2.749	2.788	3.019	3.019	2.963	3.256	3.275	3.026
Cl7				3.019	3.019	2.963	3.256	3.275	3.036
Cl8				3.019	3.019	2.9634	3.579	3.560	3.909
Cl9							3.579	3.560	3.914

The symbol “Cl i ” stands for the i th chlorine ligands in the first coordination (see Fig. 5.1 for the definition of atomic labels). Those columns entitled as “Exp.” contain the experimental data of the cation-chlorine bond lengths in the pure hosts

Introduction of an impurity ion also produces local changes of the electron-density distribution, which can be evaluated by comparison of the calculated effective Mulliken charges of the crystal-lattice ions before and after doping (Table 5.6).

The Mulliken charge calculations indicate an increasing degree of covalency for $M\text{Cl}_2$ crystals when M changes along the Ca–Sr–Ba series due to the decreasing effective charge of M cation. The Tm^{2+} effective charge is in all three hosts slightly greater than the charge of the substituted ion, which causes then a slight increase of the charge of the surrounding chlorine ions to maintain the local charge balance. It can be also noticed that the effective charges of all ions are different from their formal charges, which indicates formation of covalent bonds between the neighboring ions. Such a covalent chemical bonding behavior has been confirmed by the analysis of the bond populations between the dopant site and its nearest chlorine ligands before and after Tm^{2+} -doping. In addition, the electron-density distributions

Table 5.6 Effective Mulliken charge $Q(e)$ of individual ion and “metal-chlorine” bond population P (milli e) in the local cluster composed of the dopant site and its nearest chlorine ligands before and after Tm^{2+} -doping in $CaCl_2$, $SrCl_2$ and $BaCl_2$ crystals

M	$CaCl_2$		$SrCl_2$		$BaCl_2$	
	Ca	Tm_{Ca}	Sr	Tm_{Sr}	Ba	Tm_{Ba}
$Q(M^{2+})$	1.630	1.658	1.498	1.738	1.403	1.739
$Q(Cl1^-)$	-0.815	-0.819	-0.749	-0.782	-0.692	-0.762
$Q(Cl2^-)$	-0.815	-0.819	-0.749	-0.782	-0.692	-0.751
$Q(Cl3^-)$	-0.815	-0.817	-0.749	-0.782	-0.692	-0.751
$Q(Cl4^-)$	-0.815	-0.817	-0.749	-0.782	-0.692	-0.783
$Q(Cl5^-)$	-0.815	-0.817	-0.749	-0.782	-0.711	-0.747
$Q(Cl6^-)$	-0.815	-0.817	-0.749	-0.782	-0.711	-0.773
$Q(Cl7^-)$			-0.749	-0.782	-0.711	-0.773
$Q(Cl8^-)$			-0.749	-0.782	-0.711	-0.699
$Q(Cl9^-)$					-0.711	-0.699
$P(M^{2+}-Cl1^-)$	23	13	25	12	-3	14
$P(M^{2+}-Cl2^-)$	23	13	25	12	-2	16
$P(M^{2+}-Cl3^-)$	23	14	25	12	-2	16
$P(M^{2+}-Cl4^-)$	23	14	25	12	5	15
$P(M^{2+}-Cl5^-)$	23	14	25	12	20	13
$P(M^{2+}-Cl6^-)$	23	14	25	12	21	13
$P(M^{2+}-Cl7^-)$			25	12	21	12
$P(M^{2+}-Cl8^-)$			25	12	15	2
$P(M^{2+}-Cl9^-)$					15	2

around the Ba^{2+} and Tm^{2+} ions occupying the same site in $BaCl_2$ are not similar but rather very different: The electrons lost by Ba atom trend to go to those chlorine ligands far away from the cation site, whereas most of the transferred electrons from the Tm atom stop in the coordination environment composed of the first seven chlorine ligands as indicated by the opposite dependences of the “metal–chlorine” bond populations on the chemical bond length for the pure and doped cases.

Finally, the changes of the electronic band structure that take place on doping are shown in Fig. 5.5.

The 4f states of the Tm^{2+} ions are clearly seen in the band gap. Because Tm^{2+} ions have 13 4f electrons, spin-polarized calculations were performed to distinguish between the spin-up and spin-down states. The band-structure diagrams from Fig. 5.5 allow for the following estimation of the position of the Tm^{2+} 4f ground state in the band gap above the top of the host’s valence band: 1.05 and 2.91 eV (spin-up and spin-down states in $CaCl_2$, respectively), 1.37 and 3.20 eV (spin-up and spin-down states in $SrCl_2$, respectively), and 1.39 and 3.12 eV (spin-up and spin-down states in $BaCl_2$, respectively).

Certain asymmetry of the spin-up and spin-down state distributions is also clearly seen in Fig. 5.6, which presents the DOS/PDOS diagrams for the Tm^{2+} -doped crystals. In the case of $SrCl_2$ (cubic crystal and O_h local symmetry around the Tm^{2+}

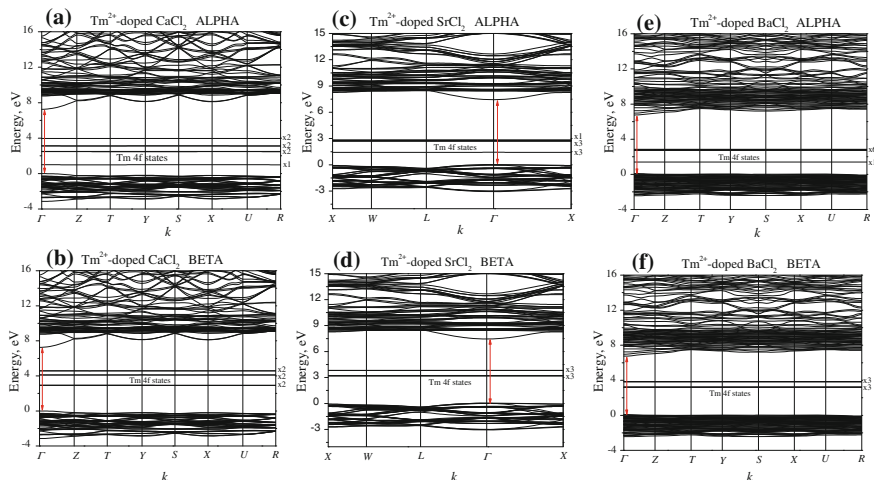


Fig. 5.5 Calculated band-structure diagrams for Tm^{2+} -doped MCl_2 [$M = \text{Ca}$ (a and b), Sr (c and d), and Ba (e and f)] crystals. The red two-way arrows indicate the energy separation between the host valence and conduction bands. ALPHA and BETA represent the electronic pictures with the up and down spins, respectively. **c, d** Adapted from Ref. [10] by permission of John Wiley & Sons Ltd

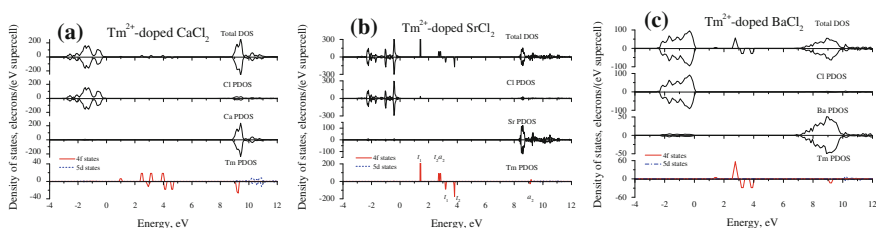


Fig. 5.6 Calculated PDOS/DOS diagrams for Tm^{2+} -doped MCl_2 [$M = \text{Ca}$ (a), Sr (b), and Ba (c)] crystals. **b** Adapted from Ref. [10] by permission of John Wiley & Sons Ltd

site), it was also possible to determine the symmetry properties of the split electron states and assign the O_h group irreducible representations as shown in Fig. 5.6.

5.6 Crystal-Field Modeling of the Tm^{2+} Spectra in SrCl_2 Crystal

As described in Sect. 5.3.2, the overlap integrals between an impurity ion and the ligands are needed to apply the ECM. These integrals, in the case of the Tm^{2+} and Cl^- ions, were calculated numerically for various Tm^{2+} - Cl^- distances. They vary smoothly with the interionic separation as shown in Figs. 5.7 and 5.8.

Fig. 5.7 Calculated dependence of overlap integrals on the distance between Tm^{2+} and Cl^- ions ($\langle 4f0|3s0\rangle$ [solid line], $\langle 4f0|3p0\rangle$ [dashed line], and $\langle 4f1|3p1\rangle$ [dash-dotted line]). Reproduced from Ref. [10] by permission of John Wiley & Sons Ltd

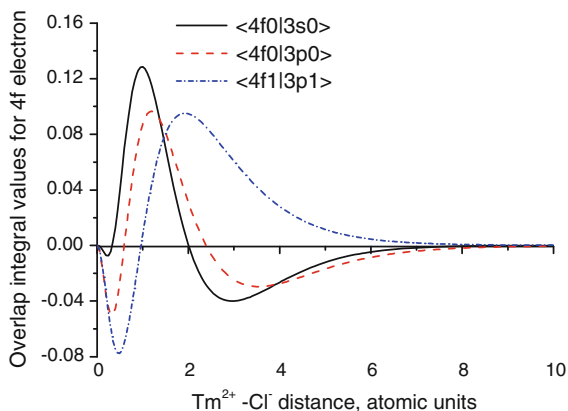
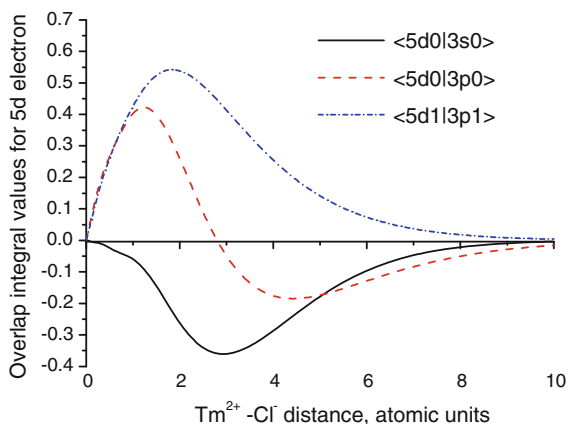


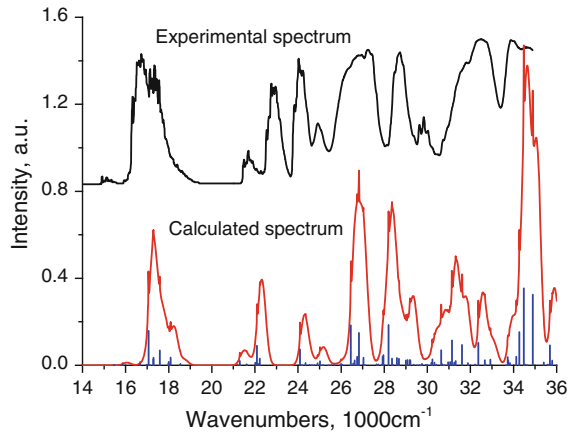
Fig. 5.8 Calculated dependence of overlap integrals on the distance between Tm^{2+} and Cl^- ions ($\langle 5d0|3s0\rangle$ [solid line], $\langle 5d0|3p0\rangle$ [dashed line], and $\langle 5d1|3p1\rangle$ [dash-dotted line]). Reproduced from Ref. [10] by permission of John Wiley & Sons Ltd



Based on the structure of the Tm^{2+} -doped SrCl_2 optimized by the first-principles calculation, the non-zero 4f and 5d CFPs of Tm^{2+} ions in SrCl_2 can be estimated as follows— $B_0^4(5d) = -18944$, $B_4^4(5d) = B_{-4}^4(5d) = -11321$, $B_0^4(4f) = -567$, $B_4^4(4f) = (4f) = -339$, $B_0^6(4f) = 340$, and $B_4^6(4f) = B_{-4}^6(4f) = -636$ (all in cm^{-1})—where the $G(4f)$ and $G(5d)$ parameter values can be fitted from the experimental 4f–4f and 4f–5d spectra [2] and are equal to 7.3 and 1.1, respectively.

With all of these parameters, it was possible to calculate the energy levels of the $4f^{13}$ and $4f^{12}5d$ electron configurations of the Tm^{2+} ions in SrCl_2 . In addition, probabilities of the electric dipole transitions between all possible states were also calculated. Finally, the simulated and measured 4f–5d spectra of $\text{SrCl}_2:\text{Tm}^{2+}$ are shown together shown in Fig. 5.9 where the pure 4f–5d transition lines are represented by the vertical bars, and the broad bands are reproduced by using the Gaussian-shaped curves with a full width at half maximum $E_{\text{width}} = 400 \text{ cm}^{-1}$,

Fig. 5.9 Experimental absorption spectrum (*top*) and simulated $4f^{13}-4f^{12}5d$ transition spectrum (*below*) for $\text{SrCl}_2:\text{Tm}^{2+}$. The *vertical bars* show the calculated locations and relative intensities of pure electronic transitions. Reproduced from Ref. [10] by permission of John Wiley & Sons Ltd



which are displaced from the zero-phonon lines by $E_{\text{shift}} = 200 \text{ cm}^{-1}$. It can be seen from Fig. 5.9 that the simulated spectrum is in good agreement with the experimental one including the positions of the absorption maxima and relative intensity of the absorption bands.

5.7 Summary

Detailed analysis of the structural and electronic properties of pure and Tm^{2+} -doped CaCl_2 , SrCl_2 , and BaCl_2 is presented in this chapter. First-principles calculations of the structural, electronic, and elastic properties were performed. Special emphasis was placed on variation of the structural and electronic properties on doping with Tm^{2+} ions. In particular, the position of the ground $4f$ level of thulium ions in the band gap of each considered material was determined. The calculated local structure of the impurity Tm^{2+} ions were applied to the understanding of the $4f-5d$ absorption spectrum of Tm^{2+} ions in SrCl_2 by employing semi-empirical CF theory. The successful theoretical simulation reveals that such a hybrid method is a good tool for describing the structural, electronic, and related optical properties of lanthanide defects in solids.

Acknowledgments C.-G. Ma acknowledges financial support from the National Natural Science Foundation of China (Grant No. 11204393), Scientific Research Foundation for the Selected Overseas Chinese Scholars, Ministry of Human Resources and Social Security of China (Grant No. 2014-167), National Training Program of Innovation and Entrepreneurship for Undergraduates (Grant No. 201410617001), Natural Science Foundation Project of Chongqing (Grant No. CSTC2014JCYJA50034), and Research Training Program for Undergraduates of Chongqing University of Posts and Telecommunications (Grant No. A2013-70). M. G. Brik acknowledges support from the European Regional Development Fund (Center of Excellence ‘Mesosystems: Theory and Applications’, TK114), Marie Curie Initial Training

Network LUMINET (Grant Agreement No. 316906), Chinese Recruitment Program of High-end Foreign Experts (Grant No. GDW20145200225), and the Programme for Foreign Experts offered by CQUPT and the Ministry of Education and Research of Estonia, Project PUT430.

References

1. Liu GK (2005) In: Liu GK, Jacquier B(eds) Spectroscopic properties of rare earths in optical materials. Tsinghua University Press & Springer (Berlin), Heidelberg, 2005, p 1
2. Grimm J, Wenger OS, Krämer KW, Güdek HU (2007) 4f-4f and 4f-5d excited states and luminescence properties of Tm²⁺-doped CaF₂, CaCl₂, SrCl₂ and BaCl₂. *J Lumin* 126:590
3. Kiss ZJ (1962) Energy levels of divalent thulium in CaF₂. *Phys Rev* 127:718
4. McClure DS, Kiss ZJ (1963) Survey of the spectra of the divalent rare-earth ions in cubic crystals. *J Chem Phys* 39:3251
5. Loh E (1968) 4fⁿ → 4fⁿ⁻¹5d spectra of rare-earth ions in crystals. *Phys Rev* 175:533
6. Sabisky ES, Anderson CH (1967) Optically induced Tm²⁺ ions in trigonal sites in BaF₂. *Phys Rev* 159:234
7. Feofilov PP, Kaplyansky AA (1962) Spectra of divalent rare earth ions in the crystals of alkali-earth fluorides. 1. Samarium. *Opt Spectr* 12:493
8. Kaplyansky AA, Feofilov PP (1962) Spectra of divalent rare earth ions in the crystals of alkali-earth fluorides. 2. Europium and ytterbium. *Opt Spectr* 13: 235
9. Duncan RC, Kiss ZJ (1963) Continuously operating CaF₂:Tm²⁺ optical maser. *Appl Phys Lett* 3:23
10. Ma CG, Brik MG (2013) First-principles calculations of structural and electronic properties of pure and Tm²⁺-doped SrCl₂. *Phys Stat Solidi B* 250:858
11. Brik MG, Sildos I, Kiisk V (2011) Calculations of physical properties of pure and doped crystals: Ab initio and semi-empirical methods in application to YAlO₃:Ce³⁺ and TiO₂. *J Lumin* 131:396
12. Brik MG, Kityk IV, Ozga K, Slezak A (2011) Structural, electronic and optical properties of pure and Ni²⁺-doped CdI₂ layered crystals as explored by ab initio and crystal field calculations. *Phys B* 406:192
13. Nazarov M, Brik MG, Spassky D, Tsukerblat B, Nor Nazida A, Ahmad-Fauzi MN (2013) Structural and electronic properties of SrAl₂O₄:Eu²⁺ from density functional theory calculations. *J Alloys Compds* 573:6
14. Anderson CH, Call P, Stott J, Hayes W (1975) Correlation between superhyperfine constants and ef crystal field parameters of Tm²⁺ in CaF₂, SrF₂, and BaF₂. *Phys RevB* 11:3305
15. Voronko YK, Larionov AL, Malkin BZ (1976) Vibrational structure of optical spectra of CaF₂:Tm²⁺, CaF₂:Yb³⁺ crystals. *Optika i Spektroskopiya* 40:86
16. Van Bever AK, Nieuwenkamp W (1935) Die Kristallstruktur von Calciumchlorid, CaCl₂. *ZKristallographie* 90:374
17. Brauer G, Müller O (1958) Zur Kristallchemie des Strontiumchlorids. *Z AnorgAllgChem* 295:218
18. Brackett EB, Brackett TE, Sass RL (1963) The crystal structures of barium chloride, barium bromide, and barium iodide. *J PhysChem* 67:2132
19. Momma K, Izumi F (2011) VESTA 3 for three-dimensional visualization of crystal, volumetric and morphology data. *J Appl Crystallogr* 44:1272
20. Dovesi R et al (2009) CRYSTAL09 user's manual. University of Torino, Torino, Italy, p 76
21. Blanca-Romero A, Berrondo M, Rivas-Silva JF (2011) Kondo-like resonance in ZnO:Eu. *IntJ Quant Chem* 111:3831
22. Demichelis R, Civalleri B, Ferrabone M (2010) Dovesi R (2010) On the performance of eleven DFT functionals in the description of the vibrational properties of aluminosilicates. *IntJ Quant Chem* 110:406

23. Li G, Lin CC, Chen WT, Molokeev MS, Atuchin VV, Chiang CY, Zhou W, Wang CW, Li WH, Sheu HS, Chan TS, Ma CG, Liu RS (2014) Photoluminescence tuning via cation substitution in oxonitridosilicate phosphors: DFT calculations, different site occupations, and luminescence mechanisms. *Chem Mater* 26:2991
24. Liu CM, Qi ZM, Ma CG, Dorenbos P, Hou DJ, Zhang S, Kuang XJ, Zhang JH, Liang HB (2014) High light yield of $\text{Sr}_8(\text{Si}_4\text{O}_{12})\text{Cl}_8\text{:Eu}^{2+}$ under X-ray excitation and its temperature-dependent luminescent characteristics. *Chem Mater* 26:3709
25. Basu M, Zhang ZW, Chen CJ, Chen PT, Yang KC, Ma CG, Lin CC, Hu SF, Liu RS (2015) Heterostructure of Si and CoSe_2 : a promising photocathode based on a non-noble metal catalyst for photoelectrochemical hydrogen evolution. *Angew Chem Int Ed* 54:6211
26. Aprà E, Causà M, Prencipe M, Dovesi R, Saunders VR (1993) On the structural properties of NaCl: an ab initio study of the B1–B2 phase transition. *J Phys Condens Matter* 5:2969
27. Valenzano L, Torres FJ, Klaus D, Pascale F, Zicovich-Wilson CM, Dovesi R (2006) Ab initio study of the vibrational spectrum and related properties of crystalline compounds; the case of CaCO_3 calcite. *Z Phys Chem* 220:893
28. Lim IS, Stoll H, Schwerdtfeger P (2006) Relativistic small-core energy-consistent pseudo potentials for the alkaline-earth elements from Ca to Ra. *J Chem Phys* 124:034107
29. Dolg M, Stoll H, Preuss H (1989) Energy-adjusted ab initio pseudo potentials for the rare earth elements. *J Chem Phys* 90:1730
30. Cao XY, Dolg M (2002) Segmented contraction scheme for small-core lanthanide pseudo potential basis sets. *J Mol Struct Theo Chem* 581:139
31. Evarestov RA (2007) Quantum chemistry of solids. Springer-Verlag, Heidelberg
32. Perger WF, Criswell J, Civalleri B, Dovesi R (2009) Ab-initio calculation of elastic constants of crystalline systems with the CRYSTAL code. *Comp Phys Comm* 180:1753
33. Reid MF, van Pieteron L, Wegh RT, Meijerink A (2000) Spectroscopy and calculations for $4f^N \rightarrow 4f^{N-1}5d$ transitions of lanthanide ions in LiYF_4 . *Phys Rev B* 62:14744
34. Duan CK, Tanner PA (2010) What use are crystal field parameters? A chemist's viewpoint. *J Phys Chem A* 114:6055
35. Wybourne BG (1965) Spectroscopic properties of rare earths. Interscience Publishers (Wiley, Inc., New York), p 164
36. Ma CG, Brik MG, Ryba-Romanowski W, Swart HC, Gusowski MA (2012) Spectroscopy and calculations for $4f^N \rightarrow 4f^{N-1}5d$ transitions of lanthanide ions in K_3YF_6 . *J Phys Chem A* 116:9158
37. Pan ZF, Ning LX, Cheng BM, Tanner PA (2006) Absorption, excitation and emission spectra of $\text{SrCl}_2\text{:Eu}^{2+}$. *Chem Phys Lett* 428:78
38. Cowan RD (1981) The theory of atomic structure and spectra. University of California Press, Berkeley, p 456
39. Ma CG, Brik MG, Tian Y, Li QX (2014) Systematic analysis of spectroscopic characteristics of the lanthanide and actinide ions with the $4f^{N-1}5d$ and $5f^{N-1}6d$ electronic configurations in a free state. *J Alloys Compds* 603:255
40. Malkin BZ, Solovyev OV, Malishev AY, Saikin SK (2007) Theoretical studies of electron-vibrational $4f^N-4f^{N-1}5d$ spectra in $\text{LiYF}_4\text{:RE}^{3+}$ crystals. *J Lumin* 125:175
41. Edvardsson S, Klintonberg M (1999) The use of CI calculated polarizabilities to study rare-earth CFP dependencies in the laser host RE:YLF. *Mater Sci Forum* 315:407
42. Sugiura C (1974) Chlorine K-x-ray spectra and electronic band structure of MgCl_2 , CaCl_2 , SrCl_2 and BaCl_2 . *Phys Rev B* 9:2679
43. Lauer HV Jr, Solberg KA, Kühner DH, Bron WE (1971) Elastic constants of EuF_2 and SrCl_2 . *Phys Lett A* 35:219
44. Kanchana V, Vaitheeswaran G, Souvatzis P, Eriksson O, Lebegue S (2010) Density functional study of the electronic structure and lattice dynamics of SrCl_2 . *J Phys Condens Matter* 22:445402

45. Kumar P, Vedeshwar AG (2015) DFT calculations of structural, electronic, optical and elastic properties of scintillator materials BaCl₂ and BaBr₂. *J Phys D Appl Phys* 48:105301
46. Nye JF (1985) *Physical properties of crystals*. Clarendon Press, Oxford, p 143
47. Shannon RD (1976) Revised effective ionic radii and systematic studies of interatomic distances in halides and chalcogenides. *Acta Crystallogr Sect A: Found Crystallogr* 32:751